ChemComm

COMMUNICATION

View Article Online
View Journal | View Issue

Cite this: *Chem. Commun.*, 2024, **60**, 12249

Received 23rd July 2024,
Accepted 23rd September 2024

DOI: 10.1039/d4cc03681f

rsc.li/chemcomm

An octahedral coordination cage with six Fe(III) centers as a T_1 MRI probe†

Aruni Dissanayake,[a] Joseph A. Spernyak [b] and Janet R. Morrow *[a]

The incorporation of multiple Fe(III) centers bridged by rigid ligands into a coordination cage represents a powerful approach for designing effective MRI contrast agents. In this context, an octahedral coordination cage with six high-spin Fe(III) centers is shown to be water soluble, robust towards dissociation and has effective relaxivity as a T_1 MRI probe in solution and in mice.

Self-assembled coordination cages show promise for the development of new classes of biomedical imaging probes.[1] Coordination cages have rigid organic linkers connecting multiple metal ion centers to give symmetrical three-dimensional shapes. The high degree of symmetry of these metal organic polyhedra may be advantageous for imaging applications that would benefit from increased signal intensity. As well-defined molecules, the properties of coordination cages may be tuned at a molecular level to produce responsive probes for molecular imaging. Coordination cages have been studied as MRI,[2,3] radiopharmaceutical[4,5] or fluorescent[6,7] probes. The scaffold of a coordination cage may itself contain the imaging probe, such as paramagnetic or luminescent metal ions incorporated into the cage. Alternatively, the organic linkers may be further appended with recognition groups or additional imaging probes. Moreover, the container-like properties of coordination cages for the encapsulation of guest molecules are a unique feature for biomedical applications.[1] Such host–guest properties are a further motivation for studying coordination cages as imaging or theranostic probes.

Our interest in coordination cages that contain biologically relevant metal ions for MR imaging applications[8,9] have led us to study iron-based cages.[2] Iron MRI probes are of interest as alternatives to Gd(III) based agents and high-spin Fe(III) complexes are of particular interest as iron is a biologically relevant metal that can be stored and recycled by the human body.[10,11] The most commonly studied Fe(III) complexes for MRI contain macrocycles or linear chelators.[8,12,13] In comparison, self-assembled iron coordination cages are a little explored but promising alternative approach to effective T_1 MRI probes. Our initial example of coordination cages for MRI featured the self-assembled Fe(III) tetrahedral cages first reported by the Raymond group ($K_{12}[Fe_4L_6]$) [L = *N*,*N*-bis(2,3-dihydroxybenzoyl)-1,5-(diaminonaphthalene)].[14] These cages contain high spin Fe(III) centers[2,14] and have the advantage of being kinetically robust towards dissociation in aqueous solution even when challenged with competing ligands such as EDTA. An added benefit is the effective proton relaxivity produced by the four tightly connected Fe(III) centers that tumble slowly in solution and the accumulation of the MRI probe in murine tumors.[2]

Additional examples of Fe(III) coordination cages with distinct polyhedral shapes and coordination spheres would add to our understanding of the factors that are important in the development of this new class of Fe(III) MRI probes.[15,16] Here we show that an octahedral Fe(III) coordination cage with six Fe(III) centers connected through four linkers (L) and containing acylhydrazone linkages forms a compound with composition of $K_6[Fe_6L_4]$ as a high relaxivity MRI probe that is very inert to dissociation. These studies were motivated by a recent report of an octahedral Ga(III) cage with acylhydrazone linkages and sulfonated phenolate donor groups which is soluble in aqueous solution.[17] Given that Ga(III) has an ionic radius and coordination sphere that is similar to that of Fe(III), we were inspired to study iron cages with this type of linker. The research described here is only the second example, to the best of our knowledge, of an iron coordination cage developed for use as a transition metal-based alternative to Ln(III) MRI probes.

The M_6L_4 cages were prepared by combining four *C*3-symmetric facial linkers formed from tris-acylhydrazide and salicylaldehyde (H_6L) and six $M(acac)_3$ where M is Fe(III) or Ga(III) (Scheme 1). Each linker contains three tridentate ligands emanating from the central aromatic group. The three donor groups are the phenolate oxygen, and the nitrogen and oxygen donors of the acylhydrazone moiety.

[a] *Department of Chemistry, University at Buffalo, The State University of New York, Amherst, NY 14260, USA. E-mail: jmorrow@buffalo.edu*
[b] *Department of Cell Stress Biology, Roswell Park Comprehensive Cancer Center, Buffalo, New York 14263, USA*

† Electronic supplementary information (ESI) available: Experimental details, spectroscopic data, relaxivity plots and data of mice MRI studies. See DOI: https://doi.org/10.1039/d4cc03681f

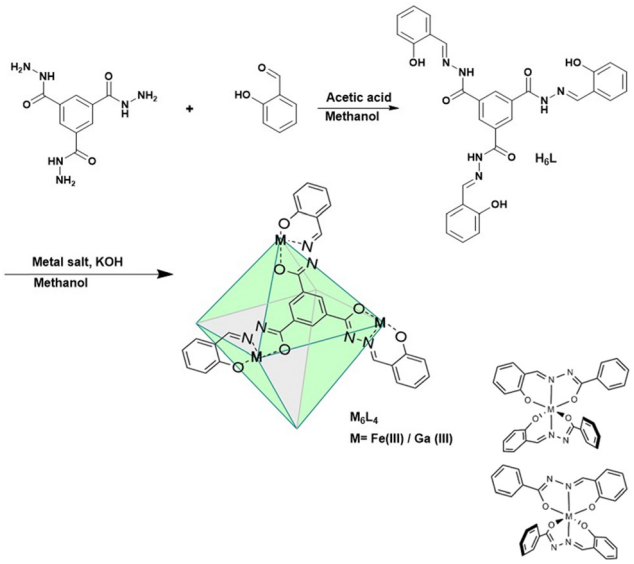

Scheme 1 Synthesis of coordination cages and configurations about metal center.

In the proposed cage structure, each M(III) binds to two of the tridentate ligands to give a six-coordinate center as shown in Scheme 1. Analogous Fe(III) bis-hydrazone or bis-semicarbazone complexes have been structurally characterized and shown to have six-coordinate centers.[18]

The diamagnetic $K_6[Ga_6L_4]$ cage was prepared initially to facilitate the use of NMR spectroscopy as a tool for characterization. The diamagnetic Ga_6L_4 cage shows six proton resonances, consistent with a highly symmetrical octahedral structure. In this octahedron, all M(III) centers are six-coordinate and bound to four oxygen donor atoms and two nitrogen donors. As noted previously for the Ga(III) cage with sulfonated phenols, there are two enantiomeric configurations of the metal center (*M* or *P* axial chirality) due to the two different arrangements of the asymmetric acylhydrazone chelate (Scheme 1).[17] If each of the six Ga(III) centers independently assumed *M* or *P* to give a cage with mixed configurations, there would be many different isomers. The presence of the simple ^{1}H NMR spectrum is consistent with a symmetrical cage with homochiral Ga(III) centers that are enantiomeric and can be designated as M_6 or P_6. The diffusion ordered spectroscopy (DOSY) plot for the Ga(III) cage is consistent with a cage radius of 1.55 nm (Fig. S6, ESI†) which compares to the sulfonated cage radius of 1.47 nm.[17] The composition of the Ga cage is further supported by high resolution mass spectrometry by electrospray ionization (HRMS-ESI) analysis. The *m*/*z* peaks that are observed at 885.0312 and 663.5220 are assigned to species with a −3 charged $[Ga_6L_4 + 3H^+]^{3-}$ and −4 charged species $[Ga_6L_4 + 2H^+]^{4-}$ with isotopic distribution patterns separated by 0.3334 ± 0.0005 and 0.2501 ± 0.0004 Dalton respectively (Fig. S8 and S9, ESI†).

The Fe(III) cage was prepared in a similar manner by addition of four equivalents of the linker, L, to six equivalents of $Fe(acac)_3$ to give Fe_6L_4. Analysis for iron is consistent with a formulation as $K_6[Fe_6(L_4)]$ which suggests that all acylhydrazones and phenol groups are fully deprotonated upon isolation

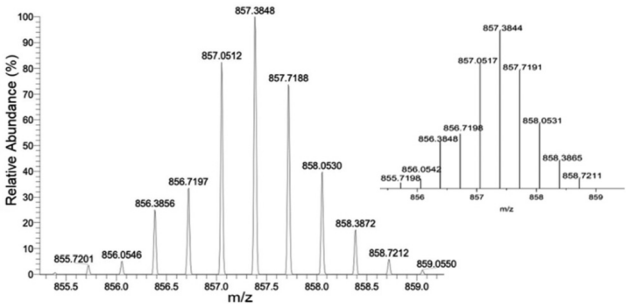

Fig. 1 HRMS-ESI of Fe_6L_4 showing observed isotopic distribution pattern for *m*/*z* = 3 − ($[Fe_6L_4 + 3H^+]^{3-}$) and theoretical isotope pattern as the insert.

of the coordination cage. Studies on bis-acylhydrazone complexes of Fe(III) also feature deprotonated acylhydrazone linkages.[18,19] A coordination cage with four fully deprotonated linkers and six trivalent metal ions would have an overall charge of negative six in solution. The ESI-HRMS spectrum of $K_6[Fe_6L_4]$ demonstrates intense peaks at *m*/*z* = 857.3848 and 642.7872 which are assigned to $[Fe_6L_4 + 3H^+]^{3-}$ and $[Fe_6L_4 + 2H^+]^{4-}$ respectively. Isotopic distribution patterns observed for the above predominant peaks follow the simulated patterns obtained based on the natural isotopic abundances (Fig. 1 and Fig. S11, ESI†).

The solution chemistry of the iron coordination cage was studied prior to investigation of the cage as an MRI probe. The water solubility of the iron-based cage is approximately 500 μM at neutral pH in PBS buffer. However, 1 mM concentrations were obtained in the presence of excess meglumine, a common additive for MRI contrast agents. The electronic absorbance spectroscopy of the iron cage in water shows a ligand to metal charge transfer (LMCT) band and several acylhydrazone-based absorbances in the UV region (Fig. S12–S17, ESI†). Monitoring of the LMCT band over time showed that the iron coordination cage stayed intact in phosphate saline buffer over 4 hours at neutral pH. Moreover, the kinetic inertness of the cage was challenged in the presence of a 10-fold excess of Zn(II) at 37 °C. The constancy of the LMCT band (Fig. S15, ESI†) is consistent with the absence of trans-metalation of the cage. Incubation of the iron coordination cage with an equivalent of EDTA also did not lead to disruption of the cage. Finally, incubation of the cage with transferrin with monitoring by UV-vis spectroscopy suggests that the cage is robust towards loss of iron to this iron storage protein.

Further characterization of the iron cage in aqueous solution shows that the Fe(III) centers are in high-spin state and stabilized as trivalent iron. Solution magnetic susceptibility measurements by Evans method gives an effective magnetic moment of 5.6 per iron, supporting high-spin Fe(III) (Fig. S18, ESI†). The ^{1}H NMR of the iron complex shows an absence of ^{1}H resonances, which is consistent with a high-spin paramagnetic center (Fig. S19, ESI†). Cyclic voltammetry studies are consistent with a stabilized trivalent Fe(III) center. The redox potential of −0.83 V *versus* NHE is sufficiently negative to maintain the trivalent state under biological conditions.[8,20]

Relaxometry studies to measure longitudinal (T_1) or transverse (T_2) relaxation of bulk water protons in the presence of the iron cage support the presence of high-spin Fe(III) centers. These centers increase proton relaxation rates (R_1 and R_2) which are normalized to 1 mM Fe(III) and are reported as r_1 and r_2 relaxivities.

The acyl hydrazone cage (Fe_6L_4) had a r_1 relaxivity of 11 mM^{-1} s^{-1} per cage (1.8 mM^{-1} s^{-1} per Fe) at 1.4 T and 34 °C, pH 7.4 in PBS buffer, whereas the Raymond cage has a r_1 of 8.4 mM^{-1} s^{-1} per cage (2.1 mM^{-1} s^{-1} per Fe) and the mononuclear complex,[21] Fe(PTOB), is 0.98 mM^{-1} s^{-1}. These data are best understood through consideration of relaxation theory.[22] Proton relaxation by paramagnetic iron centers is mediated by interaction with water molecules, predominantly through magnetic dipolar interactions.[15,22] Water molecules may be directly bound (IS, inner-sphere), associated with ligands (SS, second-sphere) or closely diffusing (OS, outer-sphere) with respect to the iron center. Dipolar coupling between paramagnetic center and water protons is modulated by correlation times including those involving electronic relaxation (τ_{1e}), water exchange (τ_m) and rotational motion (τ_R). Notably, the Fe(III) complexes listed in Table 1 lack an inner-sphere water molecule as shown by variable temperature ^{17}O NMR studies.[2,21] Analogous studies on Fe_6L_4 (Fig. 2) suggest that the transverse ^{17}O relaxation r_2° is similar to that of Fe(DTPA), which lacks an IS water rather than to Fe(CDTA) with an exchangeable IS water (Fig. 2).

The r_1 relaxivity of the coordination cages is remarkably high per iron center for a probe that acts through SS or OS water only. In comparison, the mononuclear complex, Fe(PTOB), has a r_1 of approximately 1 mM^{-1} s^{-1}, which is typical for closed coordination Fe(III) centers.[8,12] An important contributing factor is undoubtably the larger size of the cages and the correspondingly slower rotational tumbling as represented by τ_R. Rigid multimeric paramagnetic chelates are predicted to produce optimal T_1 probes at 1.5–9.4 T.[23] To further probe the mechanism of water proton relaxation by Fe_6L_4,[22] the pH dependence of r_1 was studied (Fig. 2). A pH dependence is observed if proton catalyzed relaxation of water molecules is an important mechanism[24,25] or if there is a change in speciation due to ionization of the complex over the pH range.[16,26] The lack of pH dependence of r_1 suggests that SS water interactions rather than proton exchange are operative and no speciation changes occur over this pH range. These data are congruent with other anionic Fe(III) complexes with phenolate groups that have strong SS water interactions.[26]

The r_1 of the Fe_6L_4 cage increases to 18 mM^{-1} s^{-1} upon addition of human serum albumin (HSA, 0.6 mM). This increase is consistent with binding of the coordination cage

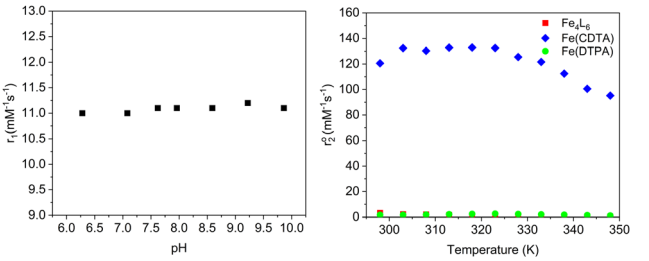

Fig. 2 The pH dependence of r_1 relaxivity of Fe_6L_4 in PBS buffer at 1.4 T, 34 °C (left). Comparison of ^{17}O NMR transverse relaxivity (r_2° per iron) for Fe_6L_4 at pH 7.5, Fe(CDTA) at pH 6.8, and Fe(DTPA) at pH 6.8 as a function of temperature (right).

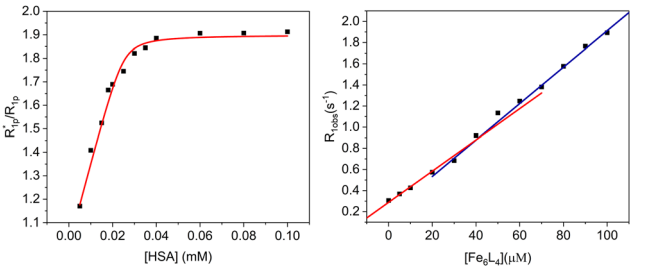

Fig. 3 E (left) and M (right) titrations of enhancement factor *versus* HSA concentration and observed relaxation rate constants as a function of cage concentration, respectively. For E titration, 100 μM Fe_6L_4 in PBS (pH 7.4) and for M titration, 10 μM HSA in PBS (pH 7.4) was used.

to serum albumin and the resultant slowing of the rotational motion of the probe. Monitoring r_1 as a function of HSA gives a binding isotherm that can be fit to a 4 : 1 stoichiometry (cage to protein) with an average association constant (K_a) of 5.4 × 10^5 M^{-1} (eqn (S5)–(S7), *E* plot, ESI†). The M plot shows a break at a 4 : 1 ratio of cage to HSA, which supports the proposed stoichiometry (Fig. 3).[27] In our case, the data fitting gives a lower limit for K_a as the binding isotherm is quite steep and the concentrations of cage probe must be in micromolar range for these measurements.

To further explore the mode of binding to HSA, the relaxivity of the iron coordination cage was studied in the presence of probes that are known to bind to the hydrophobic pockets of the serum protein including ibuprofen, iodipamide, methyl orange, warfarin or 1,3,6-trisulfonic acid (HTPS).[28] None of these competitive binders at 0.6 mM produced a change in the relaxivity of the cage, consistent with binding being predominantly electrostatic in nature.[28] However, it is possible that the competitive binders, although present in 8-fold excess, cannot effectively compete with the cage for serum albumin binding pockets. To further

Table 1 Water proton relaxivity values for Fe(III) complexes[a]

Complex	r_1 (mM^{-1} s^{-1})	r_1 (mM^{-1} s^{-1}) with HSA	r_2 (mM^{-1} s^{-1})
Fe_6L_4	11.1 ± 0.3 (1.8 per Fe)	18.0 ± 0.2 (3.0 per Fe)	14.7 ± 1.0 (2.4 per Fe)
Fe_4A_6[b]	8.3 ± 0.3 (2.1 per Fe)	26 ± 0.1 (6.5 per Fe)	—
Fe(PTOB)[c]	0.98 ± 0.05	1.4 ± 0.07	1.2 ± 0.2

[a] Measured at pH 7.4, 1.4 T, 34 °C. [b] Ref. 2. [c] Ref. 21 where PTOB is (2*S*,2′*S*)-1,1′-(7-(2-hydroxybenzyl)-1,4,7-triazonane-1,4-diyl)bis(propan-2-ol).

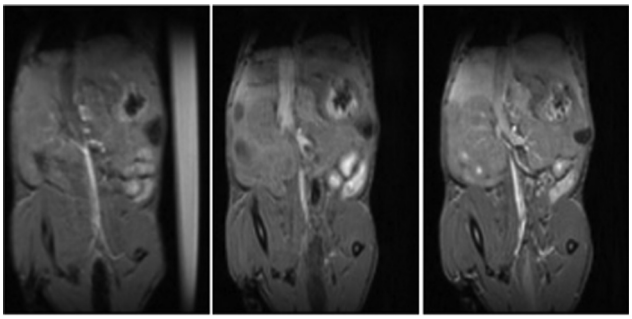

Fig. 4 T_1-Weighted MR images of BALB/c mice upon injection of 10 μmol kg^{-1} cage Fe_6L_4. Vascular enhancement is observed from pre-injection (left) to 50-minute post-injection (right). MR image collected at 5-minute post-injection is at the middle.

test for electrostatic interactions, the relaxivity of the cage was tested upon addition of poly-L-lysine, a protein of cationic charge. The relaxivity increase from 11 mM^{-1} s^{-1} to 13 mM^{-1} s^{-1} suggests that electrostatic interactions contribute to binding of the MRI probe.

The Fe_6L_4 cage was injected into BALB/c mice at 10 μmol kg^{-1} cage (60 μmol iron kg^{-1}) and monitored by T_1 weighted MRI studies over 5–50 minutes (Fig. 4 and Fig. S25–S27, ESI†). There is enhanced contrast in the vena cava over this period suggesting that the cage acts as a blood pool agent, which is consistent with its strong binding to serum albumin. Pharmacokinetic clearance is mostly through the hepatobiliary system as supported by the enhanced contrast in liver compared to bladder over time (Fig. S25–S28, ESI†). Analogous data for gadoterate meglumine is shown at 50 μmol kg^{-1} to clearly visualize the differences between the blood pool behavior of the iron coordination cage in comparison to gadoterate as an example of a hydrophilic extracellular matrix contrast agent.

In summary, an octahedral Fe(III) cage has been prepared as one of the first examples of an effective T_1 MRI probe based on a self-assembled coordination cage. The combination of four oxygen donors and two nitrogen donors in the acylhydrazone framework stabilizes high-spin Fe(III) centers in the trivalent state to give a cage which is remarkably inert towards phosphate anions, EDTA, Zn(II) or transferrin. The high relaxivity of the coordination cage as shown by a r_1 of 1.8 mM^{-1} s^{-1} for each Fe(III) center or 11 mM^{-1} s^{-1} per molecule demonstrates the power of this approach. Coordination cages are especially promising for the development of high relaxivity probes based on Fe(III) because this approach makes it feasible to produce high relaxivity probes without inner-sphere water ligands. Fe(III) complexes with inner-sphere water ligands often ionize to form hydroxide or bridging oxide ligands with a concomitant decrease in the relaxivity of the probe.[16]

A. Dissanayake: data curation, writing, analysis. J. Spernyak: writing, data curation and analysis. J. Morrow: writing, methodology, supervision, project administration.

JRM thanks the NSF (CHE-2400128) for support of this work. J. A. S. is partially supported by Roswell Park's NIH P30 grant (CA016056). This work utilized a Bruker 500 MHz NMR (NSF CHE-2018160), ICP-MS and FTMS (NSF CHE-0959565) and a preclinical MRI scanner (NIH S10D030397).

Data availability

The data supporting this article have been included in the main article and as part of the ESI.†

Conflicts of interest

JRM is a cofounder of Ferric Contrast, a company that develops iron-based contrast agents.

References

1 G. Moreno-Alcantar and A. Casini, *FEBS Lett.*, 2023, **597**, 191–202.
2 G. E. Sokolow, M. R. Crawley, D. R. Morphet, D. Asik, J. A. Spernyak, A. J. R. McGray, T. R. Cook and J. R. Morrow, *Inorg. Chem.*, 2022, **61**, 2603–2611.
3 C. He, X. Wu, J. C. Kong, T. Liu, X. L. Zhang and C. Y. Duan, *Chem. Commun.*, 2012, **48**, 9290–9292.
4 B. Woods, R. D. M. Silva, C. Schmidt, D. Wragg, M. Cavaco, V. Neves, V. F. C. Ferreira, L. Gano, T. S. Morais and F. Mendes, *et al.*, *Bioconjugate Chem.*, 2021, **32**, 1399–1408.
5 B. P. Burke, W. Grantham, M. J. Burke, G. S. Nichol, D. Roberts, I. Renard, R. Hargreaves, C. Cawthorne, S. J. Archibald and P. J. Lusby, *J. Am. Chem. Soc.*, 2018, **140**, 16877–16881.
6 Y. Qin, X. Chen, Y. Gui, H. Wang, B. Z. Tang and D. Wang, *J. Am. Chem. Soc.*, 2022, **144**, 12825–12833.
7 O. Zava, J. Mattsson, B. Therrien and P. J. Dyson, *Chem. – Eur. J.*, 2010, **16**, 1428–1431.
8 E. A. Kras, E. M. Snyder, G. E. Sokolow and J. R. Morrow, *Acc. Chem. Res.*, 2022, **55**, 1435–1444.
9 J. R. Morrow, J. J. Raymond, M. S. I. Chowdhury and P. R. Sahoo, *Inorg. Chem.*, 2022, **61**(37), 14487–14499.
10 E. C. Theil, *Inorg. Chem.*, 2013, **52**, 12223–12233.
11 A. Sargun, A. L. Fisher, A. S. Wolock, S. Phillips, M. Sojoodi, S. Khanna, J. L. Babitt and E. M. Gale, *J. Am. Chem. Soc.*, 2023, **145**, 6871–6879.
12 N. Kuźnik and M. Wyskocka, *Eur. J. Inorg. Chem.*, 2016, 445–458.
13 A. Gupta, P. Caravan, W. S. Price, C. Platas-Iglesias and E. M. Gale, *Inorg. Chem.*, 2020, **59**, 6648–6678.
14 D. L. Caulder, C. Bruckner, R. E. Powers, S. Konig, T. N. Parac, J. A. Leary and K. N. Raymond, *J. Am. Chem. Soc.*, 2001, **123**, 8923–8938.
15 Z. Baranyai, F. Carniato, A. Nucera, D. Horvath, L. Tei, C. Platas-Iglesias and M. Botta, *Chem. Sci.*, 2021, **12**, 11138–11145.
16 R. Uzal-Varela, F. Lucio-Martinez, A. Nucera, M. Botta, D. Esteban-Gomez, L. Valencia, A. Rodriguez-Rodriguez and C. Platas-Iglesias, *Inorg. Chem. Front.*, 2023, **10**(5), 1633–1649.
17 G. Wu, Y. Chen, S. Fang, L. Tong, L. Shen, C. Ge, Y. Pan, X. Shi and H. Li, *Angew. Chem., Int. Ed.*, 2021, **60**, 16594–16599.
18 D. Palanimuthu, Z. X. Wu, P. J. Jansson, N. Braidy, P. V. Bernhardt, D. R. Richardson and D. S. Kalinowski, *Dalton Trans.*, 2018, **47**, 7190–7205.
19 J. X. Yu, V. D. Kodibagkar, L. Liu, Z. W. Zhang, L. Liu, J. Magnusson and Y. T. Liu, *Chem. Sci.*, 2013, **4**, 2132–2142.
20 D. J. Kosman, *J. Biol. Chem.*, 2010, **285**, 26729–26735.
21 E. A. Kras, R. Cineus, M. R. Crawley and J. R. Morrow, *Dalton Trans.*, 2024, **53**, 4154–4164.
22 J. Wahsner, E. M. Gale, A. Rodriguez-Rodriguez and P. Caravan, *Chem. Rev.*, 2019, **119**, 957–1057.
23 P. Caravan, C. T. Farrar, L. Frullano and R. Uppal, *Contrast Media Mol. Imaging*, 2009, **4**, 89–100.
24 M. Boccalon, L. Leone, G. Marino, N. Demitri, Z. Baranyai and L. Tei, *Inorg. Chem.*, 2021, **60**, 13626–13636.
25 I. M. Carnovale, M. L. Lolli, S. C. Serra, A. F. Mingo, R. Napolitano, V. Boi, N. Guidolin, L. Lattuada, F. Tedoldi and Z. Baranyai, *Chem. Commun.*, 2018, **54**, 10056–10059.
26 A. Nucera, F. Carniato, Z. Baranyai, C. Platas-Iglesias and M. Botta, *Inorg. Chem.*, 2023, **62**, 4272–4283.
27 S. Aime, M. Botta, M. Fasano, S. G. Crich and E. Terreno, *J. Biol. Inorg. Chem.*, 1996, **1**, 312–319.
28 R. Stefania, L. Palagi, E. Di Gregorio, G. Ferrauto, V. Dinatale, S. Aime and E. Gianolio, *J. Am. Chem. Soc.*, 2023, **146**, 134–144.

